THE ROTATION RATE AND SURFACE TEMPERATURE OF THE HOT, ACCRETING WHITE DWARF IN THE DWARF NOVA RX ANDROMEDAE

Edward M. Sion
F. H. Cheng
Department of Astronomy and Astrophysics
Villanova University
Villanova, PA 19085

Paula Szkody
Department of Astronomy
University of Washington
Seattle, WA 98195

Boris Gaensicke
Universitat-Sternwarte
Göttingen 37083
Germany

C. La Dous
Webergasse 21
D-96450 Coburg
Germany

B. Hassall
Dept. of Physics, Astronomy and Mathematics
University of Central Lancashire
Preston, PR1 2HE
England

Presented at the 89th Spring Meeting of the AAVSO, April 15, 2000

Abstract

We obtained Hubble GHRS phase-resolved spectroscopic observations of the dwarf nova RX Andromedae at three times in its outburst cycle: (1) near the end of an extraordinarily deep and long dwarf nova quiescence, 3 months after the last previous outburst; (2) during the rise to outburst; and (3) near the end of a decline from outburst. The spectral wavelength range covered was 1149Å to 1435Å. All of the spectra are dominated by absorption lines with weak to moderately strong emission wings due to the continued presence of disk material. Uncertainities in line velocities preclude a K_1 determination or mass information. Our best fitting model yielded T_{wd} /1000 = 34.0 ±0.1K, log g = 8.0 ±0.1, and V_{rot} = 600 $^{+200}_{-100}$ km/s. The T_{eff} value is very similar to the T_{eff} of the white dwarf in U Gem, but the rotational velocity appears to be higher than U Gem's value. We report approximate subsolar chemical abundances of Carbon and Silicon for RX And, with C being 0.05 x solar and Si = 0.1 x solar while other elements are at essentially their solar values. However, accurate abundances are complicated by line emission and we cannot exclude that the abundances of all species are essentially at the solar values. We see no evidence of thermonuclear-processed abundance ratios. If the white dwarf mass is 0.8 $M_\odot$ (Ritter 1999), then the

corresponding white dwarf cooling age, 4 x 10^6 years, is a lower limit to the age of this CV. If the peculiar line features seen in the spectrum on the late decline from outburst are inverse P Cygni in nature, then infall velocities of ~2000km/s are indicated during the decline from outburst. We compare the surface properties of the RX And white dwarf with the properties of other CV degenerates studied to date with HST, HUT, and IUE.

1. Introduction

RX And is one of seven dwarf novae with exposed white dwarfs observed with HST during quiescence. It is the only other HST-observed system besides U Gem, lying above the period gap where the white dwarfs appear to be hotter than in CVs below the gap (Sion 1999). On average, the mass transfer rates and the evolutionary ages of CVs above the period gap are higher and lower by an order of magnitude, respectively, than of CVs below the gap (King 1988; Kolb and Stehle 1996).

A synthetic spectral analysis of the white dwarf in this system offers further insights into the physics of accretion and the response of the white dwarf to heating and injection of accreted matter with angular momentum. Among our goals in securing orbital phase-resolved GHRS G140L observations near the quadratures of its orbit during quiescence were the following: (1) the white dwarf rotation rate; (2) the T_{eff}, log *g*, and chemical abundances of the white dwarf; (3) the orbital velocity semi-amplitude K_1 and hence the white dwarf mass independent of disk emission line velocities and; (4) the cooling response of the white dwarf to compressional and irradiative heating by the dwarf nova event (Pringle 1988; Sion 1995).

The underlying white dwarf in RX And was first detected during RX And's quiescence by Holm *et al.* (1991) using an IUE low resolution SWP spectrum. Although this spectrum was dominated by emission lines due to the accretion disk, Holm *et al.* fitted a pure hydrogen log g = 8 white dwarf model atmosphere to the Lyman-α profile (with its obvious turnover) and the white dwarf continuum, yielding a temperature estimate of T_{eff} = 35,000K.

As we describe below, with an extraordinary stroke of good fortune and a study of AAVSO archival data (Mattei 1997), we obtained a spectrum at the end of an anomalously deep and unusually long quiescent interval for RX And (hereafter spectrum 1), as well as spectra during the rise to outburst (spectrum 2), and the late decline from outburst (spectrum 3). Spectrum 1 manifests the strongest evidence of the far-UV contribution of the underlying white dwarf accretor and represents the least disk-affected of any previously obtained far-UV spectrum of RX And. The results of our analysis of the white dwarf are presented below.

2. HST GHRS far ultraviolet observations

Timing HST observations to occur during a quiescence of RX And required considerable planning. AAVSO records reveal that the outbursts of RX And range from 3 to 10 days while its quiescence ranges from 5 to 20 days (Ritter 1999). The short timing of the cycle prohibited any target of opportunity status with HST. Defining a cycle length of RX And as one outburst + one quiescence, the shortest cycle length was 8 days and the longest cycle length 30 days, yielding an average cycle length of 19 days. Our observing strategy was to obtain three spectra, with the second spectrum following the first by 9.5 days and the third spectrum spaced from the second by 9.5 days. We estimated from long term AAVSO data that there was a 34% probability that the first observation would take place in outburst and 66% probability that the first spectrum would be in quiescence. This strategy gratifyingly succeeded.

The temporal placement of the observations with respect to the outburst and quiescence cycle of RX And is shown in Figure 1 where we present the AAVSO light

curve data. The first set of observations took place approximately 110 days after the last previous outburst, the second set during the rise to outburst, and the third set on the decline from outburst. Since it is the first spectrum (with the lowest flux level) where we have optimal exposure of the white dwarf, it is the primary focus in this study. Spectrum 2 is disk-dominated, while spectrum 3 is affected by the accretion disk but less so than spectrum 2, which was obtained on the rise to outburst. Spectra 2 and 3 will undergo more detailed analysis in conjunction with the IUE archival spectra on the middle rise and late decline from outburst of RX And and will be reported in a followup paper (La Dous *et al.* 2000).

The observations for spectra 1, 2, and 3 were carried out in the ACCUM mode through the large science aperture (2.0) with the D1 detector of GHRS and the G140L disperser. The wavelength coverage was 1149Å to 1435Å with a spectral resolution of 0.6Å. The resulting spectra have a signal-to-noise ratio of 15–20:1 over most of the covered wavelength range. The observations are presented in heliocentric time and velocity in Table 1, where we have listed the start time of the observations, the total exposure time in seconds, and the orbital phase at the start and end of the total exposure. Heliocentric time corrections were included in the phasing.

The orbital phase range in Table 1 was computed by using the best available orbital ephemeris due to Kaitchuk (1989), where phase 0 = HJD 2447041.932 ± 0.002 +0.2098930E ± 0.0000001. In this phase convention, the white dwarf would have maximum positive velocity at phase 0.75 and maximum negative velocity at phase 0.25. Since a major objective of our line formation study was to delineate white dwarf lines by their velocity, and obtain mass information for the white dwarf, we required observations close to the quadrature points of the orbit.

Table 1. HST GHRS Observations of RX And.

Obs. No.	*Obs. date* *Obs. time*	*Total Exp.* *(sec)*	ϕ *(start)*	ϕ *(end)*
1	1996/12/22 11:03:06	1414	0.35	0.43
2	1997/01/09 11:41:52	1142	0.23	0.29
3	1997/01/20 06:33:20	1142	0.61	0.68

The absorption lines seen in the three spectra of RX And have their origin in the interstellar medium, the white dwarf, or the accretion disk. First, we discuss the narrow interstellar lines detected in the spectrum of RX And. These lines are particularly well-detected in spectrum 2 due to the higher signal-to-noise ratio. Measuring the wavelengths of the strongest interstellar lines (Si II 1260, O I 1302, Si II 1304, C II 1334, C*II 1335) indicates that the wavelength zeropoints in spectra 2 and 3 are offset by -0.4Å, while a marginal offset of -0.1Å is determined for spectrum 1. Shifting the interstellar lines to zero velocity allows us to correct the wavelength scale. Additional interstellar absorption features of Si II 1190/93/94 and N I 1200 might be present in the spectra, but cannot be reliably detected at the given S/N.

The summed spectrum 1, displayed in Figure 2 (top panel), reveals a spectrum dominated by absorption, in some cases flanked by weak to moderately strong emission wings. The Stark-broadened Lyman-α profile is clearly present. The emission suggests some disk contribution even at the end of the anomalously long quiescence. However, we emphasize that spectrum 1 is unlike any other ever obtained during a quiescence of RX And with any orbiting far ultraviolet telescope.

In spectrum 1, the strongest lines associated with the white dwarf besides Lyman-α are C III 1175, N V 1238/42, Si III 1298, possibly O VI 1343, and Si IV 1393/1403. All these absorption features have positive velocities in the range of ~80 to 230 km/s, with the highest velocities at N V (1238, 1242). However, the N V values are also the most unreliable ones, due to strong blending by the emission line. We cannot rule out that N V is from a hotter boundary layer area or of coronal origin, as in U Gem during its quiescence (Sion *et al.* 1998).

In Figure 2 (middle panel), the summed spectrum 2 is displayed. This spectrum resembles the outburst spectrum of U Gem (see Sion *et al.* 1997). We see a factor of 3 higher flux level than during the deep low state corresponding to spectrum 1, with strong broad absorption lines dominating, while emission features are absent. In this spectrum, obtained on the rise to outburst, all of the strong absorption lines have a velocity ~+100 km/s, with the exception of C III 1175, which is at only ~50 km/s. All of the strong absorption features are extremely broad, almost certainly the result of Keplerian motion associated with the inner accretion disk. Note that the broad Si II 1260, 1265 absorption must originate in colder parts of the disk since we do not believe the white dwarf is exposed on the rise to outburst. Since the white dwarf during this intense accretion phase can only be hotter than it was when spectrum 1 was obtained, the Si II 1260, 1265 features cannot be of white dwarf origin since they were not seen in spectrum 1. All of the interstellar lines are at their rest wavelength. The Si II 1260, O I 1302, and Si II 1304 are particularly prominent in spectrum 2.

Figure 2 (bottom panel) displays spectrum 3, which was obtained during the late decline from outburst. This spectrum is dominated by absorption features with emission wings. Curiously, several features are seen with a red asymmetric profile and steep emission on the blue side, resembling inverse P Cygni profiles (see below). In spectrum 3, all of the strong absorption lines have negative velocities in the range ~-80 to -150 km/s, with C III having the lowest (least negative) velocity.

In summary, the line velocities indicate that spectrum 1 has 4 lines (C III 1175, N V 1238, 1242, O IV 1343, and Si IV 1393, 1402) with large positive velocities, spectrum 2 has fewer positive velocities, and spectrum 3 has three lines with large negative values (C III, N V, Si IV). These lines, with the largest displacements in spectrum 1 and spectrum 3, may originate in the white dwarf or its associated boundary layer. Unfortunately, the velocity signs are directly opposite to what is expected from our adopted phasing, *i. e.*, phase 0 corresponds to inferior conjunction of the secondary. Therefore, the white dwarf should have maximum positive velocity at phase 0.75 (closest to spectrum 3) and maximum negative velocity at phase 0.25 (spectrum 2). We attribute the deviation of the measured velocities from the expected values at each phase to the presence of line blends and asymmetric (and peculiar) profile shapes. The effect of the ''outbursting'' disk in spectra 2 and 3 may be affecting the gamma velocity, as is the case in superoutbursts of SU UMa systems (Vogt 1983), creating the very negative gamma velocity seen in spectrum 3. However, we note that the ephemeris due to Kaitchuck (1989) has not been subjected to any other modern-day test of its validity. In summary, it is not possible to obtain a reliable value of K_1 or the white dwarf mass from the three HST summed spectra.

3. Synthetic spectral fitting

In order to model spectrum 1 of RX And and estimate the white dwarf properties during quiescence, we constructed a grid of model stellar atmosphere spectra under local thermodynamic equilibrium (LTE) with TLUSTY195 (Hubeny 1988; Hubeny and Lanz 1995) and SYNSPEC42 (Hubeny *et al.* 1994), initially with solar abundance.

In preparation for our discretized χ^2 minimization fitting procedure, we also masked the following wavelength regions to exclude strong emission line

contributions: 1209Å–1220Å, 1236Å–1248Å, 1336Å–1346Å, and 1381Å–1400Å. We constructed a three-parameter grid of models with varying V_{rot}, log *g*, and T_{wd}. The parameter ranges are V_{rot} = 0, 100, 200,...1000 km/s, log *g* = 7.5, 8.0, 8.5, 9.0, and T_{wd} /1000 = 31, 32,....40 K. A total of 440 models were created. In order to keep the number of free parameters as small as possible, we applied no correction for reddening, which is most likely very low (Verbunt 1987). Our best fitting model (with a redward shift of 3Å and a reduced χ^2 of 3.1066) yielded T_{wd} /1000 = 34.0 ±0.1 K, log *g* = 8.0 ±0.1, and $V_{rot} = 600\ ^{+200}_{-100}$ km/s.

As the temperature and gravity determination is driven in large part by the observed Lyman-α absorption profile, it is necessary to estimate the correlation between these two parameters. The width of the Lyman-α profile increases with higher surface gravity (pressure) while it decreases for higher temperatures due to the higher degree of H ionization. In the case of RX And, this anti-correlation between T_{eff} and log *g* results in an additional uncertainty of the temperature, ~3000K, for a fixed log *g*.

The parameters of our best fit yield an optical magnitude of 16.6, a value significantly below the observed optical magnitude. This would imply that the disk dominates the optical range even in quiescence. The distance derived from the best fit scaling factor of the model spectra is d = 200 pc for $M_{wd} = 0.8M_{\odot}$. This value agrees with the estimate given by Patterson (1984).

Unfortunately, the chemical abundances are highly uncertain because the emission lines likely fill in part of the white dwarf absorption, thus causing the observed absorption strength to mimic lower abundances. In order to illustrate the effect of the observed emission line on the derived abundances, we employed an alternative approach. Again, spectrum 1 is fitted with white dwarf model spectra, but this time we use all the available wavelength range (excluding only the geocoronal Lyman-α emission), and we allow for Gaussian emission line shapes for N V, Si III, C II, Si IV. A fit consistent with the one achieved by masking the emission line regions can be obtained when the abundances are solar for all elements.

4. Concluding remarks

Our results on the RX And white dwarf offer a comparison with the properties of other CV degenerates. With T_{eff} = 34,000K, it is among the hottest CV degenerates. RX And has a temperature similar to the U Gem degenerate but a moderately faster rotation rate. These two objects are the only long-period dwarf novae with reliable surface temperature information from HST analyses. Any abundance information from spectrum 1 must be viewed with caution for the reasons stated earlier. The atmospheric abundances of C and Si in RX And are likely close to solar but modestly subsolar abundances from this spectrum cannot be excluded. We do not see evidence of surface abundance ratios indicative of past CNO processing, as we found for the white dwarfs in VW Hydri and U Gem. The rotation rate of the RX And white dwarf places it in the middle range of the presently known V sin *i* distribution. Taking the mass of the white dwarf cited in Ritter (1999) at face value, the cooling age of the white dwarf is only 4 x 10^6 years (a lower limit to the age of RX And as a CV, in the absence of core mass loss). The line velocities corresponding to the photosphere of the white dwarf could not be measured with sufficient precision to determine a K_1 velocity semi-amplitude, due to peculiar line shapes, line blends, and disk emission contamination. Therefore, we are unable to determine a reliable K_1 and gravitational redshift mass for the white dwarf.

Some of the line features in spectrum 3 appear to be longward-asymmetric (*i.e.*, asymmetric on the "red'' side) with emission on the shortward side. The impression is that disk material during the decline of the outburst has a net inward flow onto the

white dwarf. If these structures do represent inverse P Cygni features, then the infall velocity of the disk-associated or outburst-associated material is ~2550 km/s. The terminal velocity derived from the C II feature is ~1800 km/s. It is possible that the "inward"-flowing gas is ejected gas which did not achieve escape during the outburst and is falling back in. This phenomenon may occur in the high-amplitude dwarf nova WZ Sge, as discussed by Liebowitz and Mazeh (1981). Similar inverse P Cygni structures were also seen in the superoutburst spectrum of VW Hyi (Huang *et al.* 1996). If the line features in the spectrum of visit 3 are really inverse P Cygni features, then they would represent the first direct detection of actual gas infall onto the white dwarf. In that case it would be possible to derive a mass accretion rate directly.

5. Acknowledgements

This research would not have been possible without the excellent technical support and rich data archive of the AAVSO. We acknowledge with gratitude the support of this work by NASA through grant GO6700.01-96A (to Villanova University) from the Space Telescope Science Institute, which is operated by the Association of Universities for Research in Astronomy, Inc., under NASA contract NAS5-26555. EMS was also supported by NSF Grant AST 99-01955 to Villanova University.

References

Holm, A. V., Lanning, H., Mattei, J., and Nelan, E. 1991, *J. Amer. Assoc. Var. Star Obs.*, **20**, 166.
Huang, M., *et al.* 1996, *Astrophys. J.*, **458**, 355.
Hubeny, I. 1988, *Comp. Phys. Commun.*, **52**, 103.
Hubeny, I., and Lanz, T. 1995, *Astrophys. J.*, **439**, 875.
Hubeny, I., Lanz, T., and Jeffery, C. S. 1994, *Tlusty and Synspec: A User's Guide*, *Newsletter on Analysis of Astronomical Spectra* (Univ. of St. Andrews).
Kaitchuck, R. H. 1989, *Publ. Astron. Soc. Pacific*, **101**, 1129.
King, A. 1988, *Quarterly J. Roy. Astron. Soc.*, **29**, 1.
Kolb, U., and Stehle, R. 1996, *Mon. Not. Roy. Astron. Soc.*, **282**, 1454.
La Dous, C., *et al.* 2000, in preparation.
Liebowitz, E., and Mazeh, T. 1981, *Astrophys. J.*, **251**, 214.
Mattei, J. A. 1997, Visual observations from the AAVSO International Database, private communication.
Patterson, J. 1984, *Astrophys. J. Suppl.*, **54**, 443.
Pringle, J. 1988, *Mon. Not. Roy. Astron. Soc.*, **230**, 159.
Ritter, H. 1999, *CV Catalogue* Preprint.
Sion, E. 1995, *Astrophys. J.*, **438**, 789.
Sion, E. M. 1999, *Publ. Astron. Soc. Pacific*, **99**, 1.
Sion, E. M., Cheng, F. H., Szkody, P., Sparks, W., Gaensicke, B., Huang, M., and Mattei, J. 1998, *Astrophys. J.*, **496**, 449.
Sion, E. M., *et al.* 1997, *Astrophys. J.*, **483**, 907.
Verbunt, F. 1987, *Astron. and Astrophys.*, **71**, 339.
Vogt, N. 1983, *Astron. and Astrophys.*, **270**, 333.

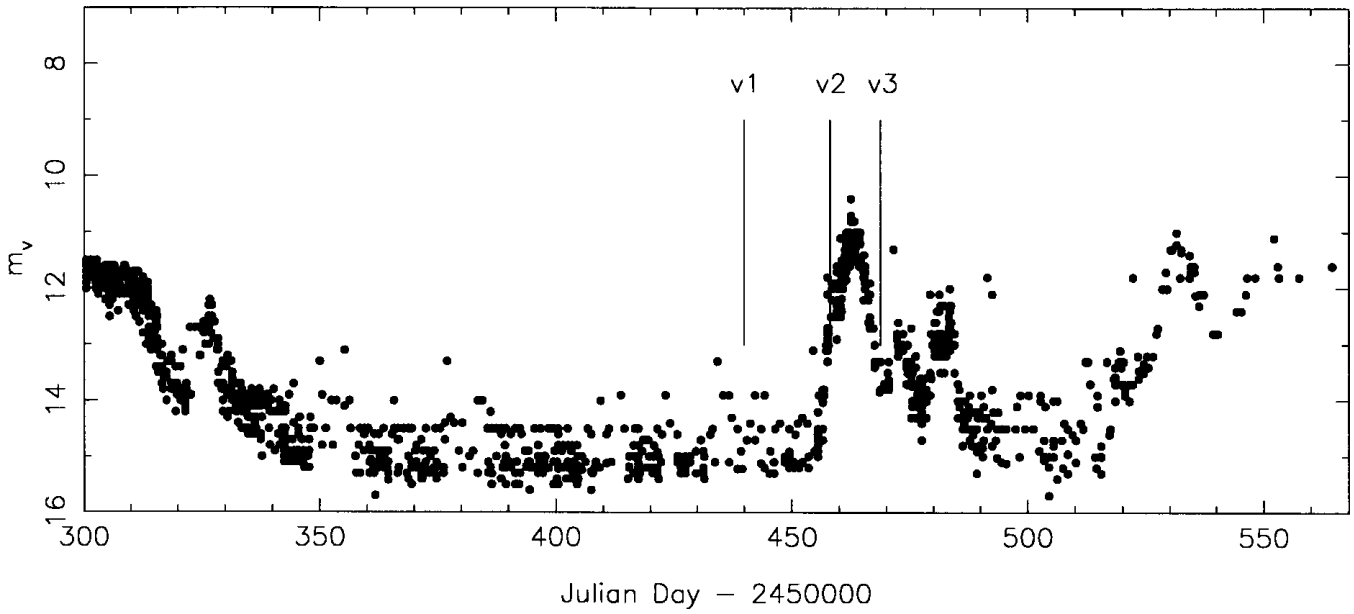

Figure 1. The AAVSO light curve for RX And during the period when the HST GHRS observations of RX And took place. The placement of the GHRS observations for each of the three visits is indicated. Note the extraordinarily long quiescent interval of RX And.

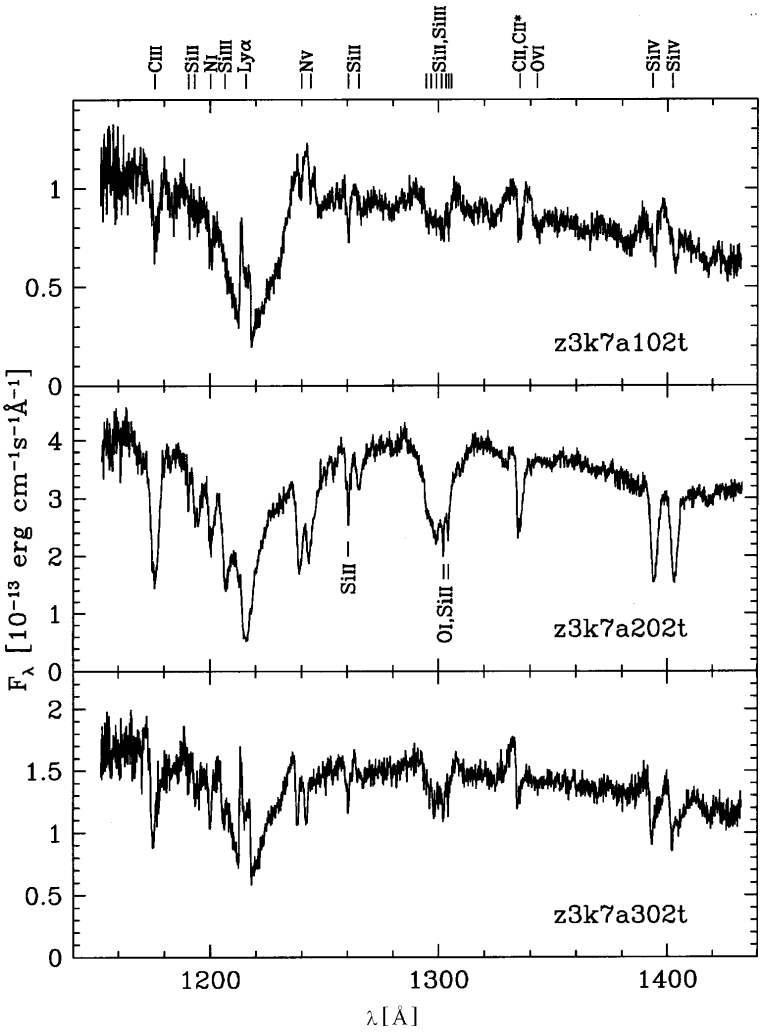

Figure 2. (top panel) The GHRS G140L spectrum of RX And (flux F_λ versus wavelength) for the first observation (late anomalous quiescence) is shown. Note the very broad Stark-broadened Lyman-α absorption with narrow airglow emission, and the rich metallic absorption line spectrum, with the strongest lines of Si II, Si III, Si IV, C II, and C III labelled in the spectrum; (middle panel) The flux F_λ versus wavelength for the second observation (rise to outburst) is shown. Note the dominance of much stronger, very broad absorption, including the great strengthening of N V and Si III. The flux level of this spectrum is the highest of the three summed spectra; (bottom panel) The flux F_λ versus wavelength for spectrum 3 (decline from outburst) is shown. Note the very broad Stark-broadened Lyman-α absorption with narrow airglow emission, and the rich but weakened metallic absorption line spectrum, with the strongest lines being Si II (1260), Si III (1298), C II (1335), and C III (1175). Note the weaker N V features and the possible longward "red'' asymmetric inverse P Cygni profiles in C III (1175), N V (1238, 1242), C II (1335), and Si IV (1393, 1402).

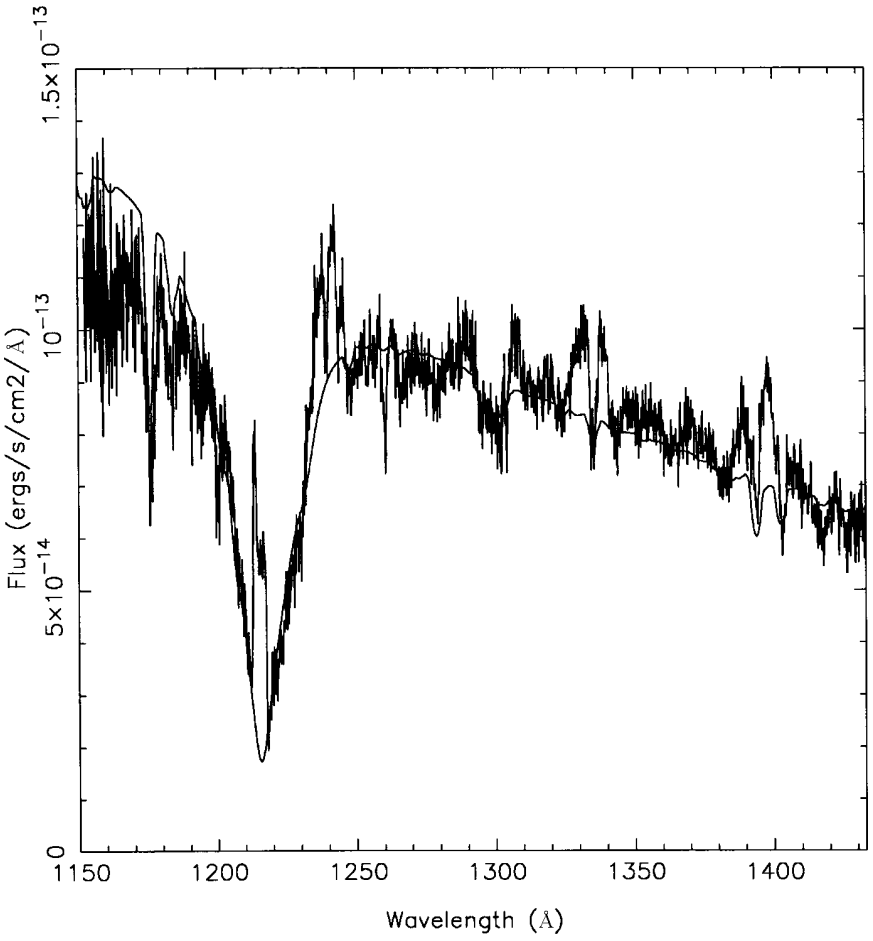

Figure 3. A comparison between the observed summed GHRS G140L spectrum (spectrum 1) of RX And in quiescence and model fit (solid line) to the GHRS data. The best fit white dwarf model yielded T_{eff} = 34,000 ±1000 K, log g = 8.0 ±0.1, and chemical abundances close to solar values.